17th International Conference on the Application of Computer
Science and Mathematics in Architecture and Civil Engineering
K. Gürlebeck and C. Könke (eds.)
Weimar, Germany, 12–14 July 2006

INVESTIGATION OF CRACK GROWTH IN POLYCRYSTALLINE MESOSTRUCTURES

T. Luther* **and C. Könke**

**Institute of Strcutural Mechanics*
Marienstrasse 15, 99423 Weimar, Germany
E-mail: torsten.luther@bauing.uni-weimar.de

Keywords: Polycrystal Model, Crack Growth Simulation, Grain Size Distribution.

Abstract. *The design and application of high performance materials demands extensive knowledge of the materials damage behavior, which significantly depends on the meso- and microstructural complexity. Numerical simulations of crack growth on multiple length scales are promising tools to understand the damage phenomena in complex materials. In polycrystalline materials it has been observed that the grain boundary decohesion is one important mechanism that leads to microcrack initiation. Following this observation the paper presents a polycrystal mesoscale model consisting of grains with orthotropic material behavior and cohesive interfaces along grain boundaries, which is able to reproduce the crack initiation and propagation along grain boundaries in polycrystalline materials. With respect to the importance of the geometry of the grain structure modeling an advanced Voronoi algorithm is proposed to generate realistic polycrystalline material structures based on measured grain size distribution. The polycrystal model is applied to investigate the crack initiation and propagation in statically loaded representative volume elements of aluminium on the mesoscale without the necessity of initial damage definition. Future research work is planned to include the mesoscale model into a multiscale model for the damage analysis in polycrystalline materials.*

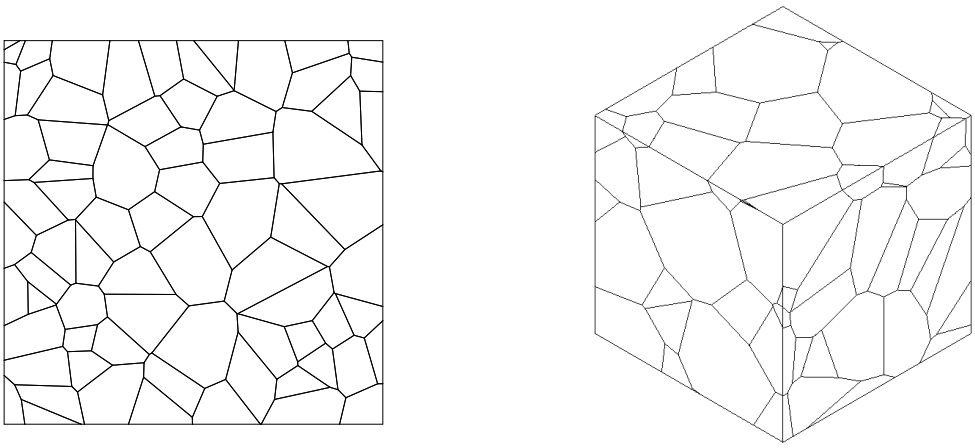

Figure 1: 'Classical' 2D and 3D Voronoi diagrams.

1 INTRODUCTION

Durability and life cycle ananlysis of engineering structures is often based on numerical simulations of macroscopic damage behavior using phenomenological damage and fracture models. Therewith the true physical mechanisms of crack initiation and various crack propagation can not be covered. In order to integrate these physical material effects simulations on the meso- or microstructure have to be performed.

For polycrystalline materials it has been observed, that grain boundary decohesion is one important mechanism that leads to crack initiation and propagation on the mesoscale (10^{-3}m-10^{-6}m) [1, 2], and which further depends strongly on atomic debonding on the microscale (10^{-6}m-10^{-10}m). The mutual dependence can be investigated by a multiscale analysis obtaining a reasonable damage model based on micro mechanical features. The current work is focused on the investigation of grain boundary depending damage behavior on the mesoscale using a two dimensional polycrystal model. Fundamentals of polycrystal modeling on mesoscale are published by Iesulauro and Ingraffea [1, 2, 3]. These publications are refered in detail in the course of geometrical generation of the polycrystal structure and assignment of material models.

In section 2 the geometrical modeling of polycrystalline mesostructure is described. Therein a modification of 'classical' Voronoi diagrams is shown to generate grain structures based on arbitrary defined grain size distributions. Section 3 gives an overview of the material models, which are assigned to grains and grain boundaries, respectively. Section 4 shows numerical results of damage analysis on representative volume elements (RVE) of aluminium on the mesoscale. In section 5 an over-all concept for the damage analysis on multiple length scales is proposed and the polycrystal model on mesoscale is arranged within the multiscale concept. Finally section 6 concludes the current work.

2 RANDOM GENERATION OF GRAIN STRUCTURE ON MESOSCALE

The application of 'classical' Voronoi algorithms [4] to generate polycrystalline material structures has become state of the art in polycrystal modeling on the mesoscale. The advantage

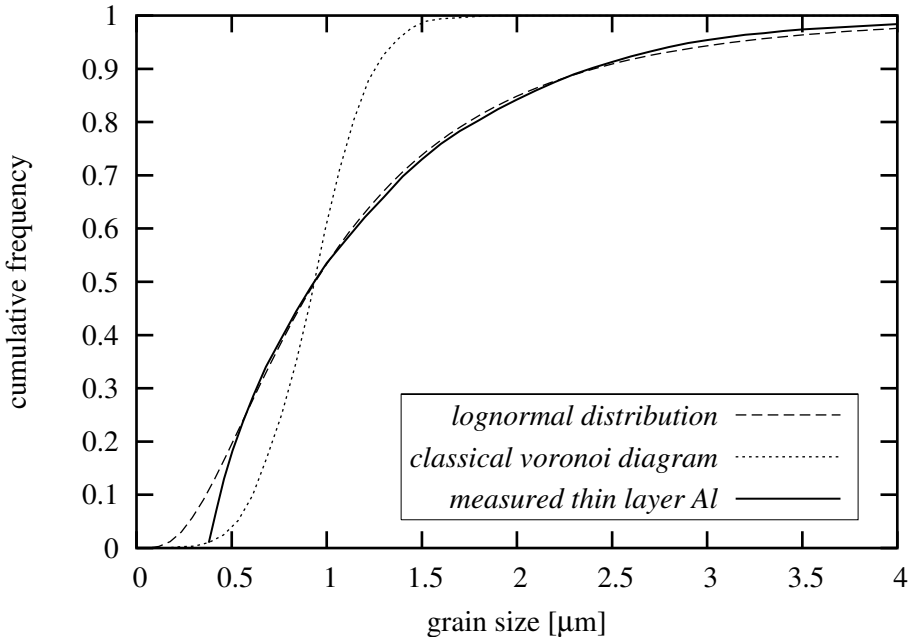

Figure 2: Cumulative grain size distribution.

of a Voronoi cell diagram (Figure 1), as applied in [1, 2, 3], is given by the simplicity of its algorithm and its random characteristics. However, 'classical' Voronoi cell diagrams are not well adapted to flexible reproduce a realistic grain size distribution in polycrystalline materials. Experimental measurements have found, that in steady state the grain size distribution is better fit by a lognormal distribution function [5, 6] or a Weibull distribution function [7]. Exemplary, Figure 2 shows cumulative grain size distribution in heat treated thin layer aluminum measured by [5] and compared to the Voronoi grain size distribution and the lognormal distribution. In grain size distribution functions the size of a single grain is defined by the diameter d of a circle with equivalent area. The plotted cumulative lognormal distribution function is computed with the measured median value $d_{50} = 0.94\mu m$ and the measured standard deviation $\sigma_d = 0.78$ [5]. The Voronoi grain size distribution was calculated by means of generated Voronoi cell diagrams with the same median value.

Based on the drawn conclusion the 'classical' Voronoi algorithm was modified to generate more realistic two dimensional grain structures of polycrystals. The concept is to predefine the size of single grains according to a specified grain size distribution and to construct a 'modified' Voronoi cell diagram considering this a priori information. In the following the lognormal distribution function $f_{LN}(d)$ is applied as starting point for the grain structure generation:

$$f_{LN}(d) = \frac{1}{\sigma_d \, d \, \sqrt{2\pi}} \, e^{-\left(\frac{1}{\sqrt{2}\,\sigma_d} ln(d/d_{50})\right)^2}, \tag{1}$$

where the median grain size d_{50} and the standard deviation σ_d are the two free distribution parameters. Alternatively a Weibull distribution $f_W(d)$ is defined by the two free distribution parameters α and β:

$$f_W(d) = \frac{\beta}{\alpha^{\beta}} \, d^{\beta-1} \, e^{-(d/\alpha)^{\beta}}. \tag{2}$$

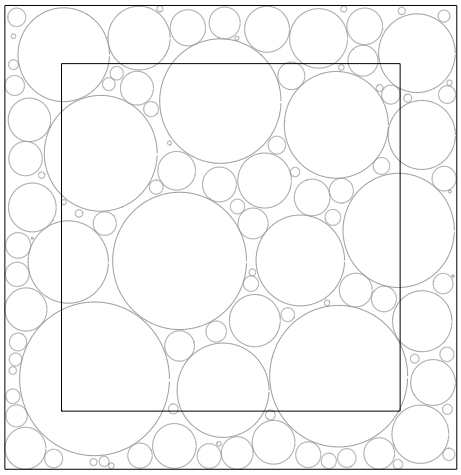

Figure 3: Circles are placed into a box (outer boundary) larger than the RVE (inner boundary).

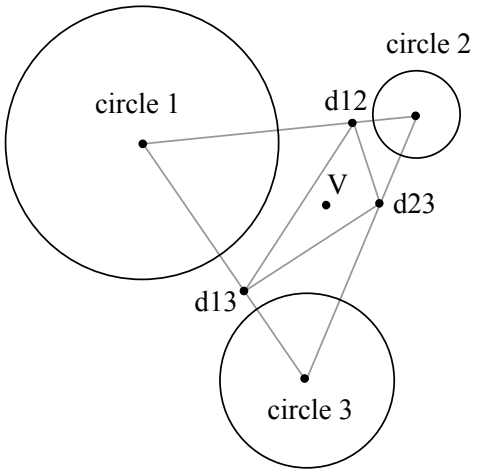

Figure 4: Construction of 'modified' Voronoi points after Delaunay triangulation.

The main advantage of the lognormal distribution function is the straightforward interpretation of its distribution parameters, which is not given in the case of Weibull distribution.

In a first step the grain structure generation starts with a random generation of diameters d according to the specified distribution function. In the case of a Weibull distribution it is possible to transform the cumulative distribution function $F_W(d)$:

$$F_W(d) = 1 - e^{-(d/\alpha)^{\beta}} \tag{3}$$

into the form:

$$d = \alpha \left\{-ln\left(1 - F_W(d)\right)\right\}^{1/\beta}. \tag{4}$$

Therewith one can find a suitable set of diameters d based on random values $0 < F_W(d) < 1$. For distribution functions, that can not be transformed into a dependency $d = d(F(d))$, e.g. the lognormal distribution, it is proposed to discretize the argument domain $0 < d \leq d_{max}$ of the distribution function $f(d)$. The discretization yields a finite number of discrete intervals $\Delta d_i = d_{i+1} - d_i$. Furthermore the probability limits $F(d_i) < F(\Delta d_i) \leq F(d_{i+1})$ are assigned to each step Δd_i according to the cumulative distribution function $F(d)$. Therewith a suitable set of diameters d based on random values $0 < F(d) \leq F(d_{max})$ can be generated.

In a second step circles with the generated diameters are defined. The circles are placed, starting with the largest one, into a box (Figure 3). The box (outer boundary) must be larger than the aimed polycrystal RVE (inner boundary) on the mesoscale to take into acount that grains at the RVE boundary can be positioned partially outside the RVE. The area, that can be filled by circles, is smaller than the box area A, because the density of circles in the box is limited. Hence, the diameter generation stops when the sum of circle areas, belonging to diameters d_j, is larger than a specified limit $f \cdot A$:

$$\sum \frac{\pi}{4} d_j^2 \geq f \cdot A\,. \tag{5}$$

The limit of Eq. 5 should be reasonable defined to guaranty, that all circles can be placed into the box. Suitable values for the factor f are between 0.7 and 0.9. However, it strongly depends on the standard deviation of grain size distribution.

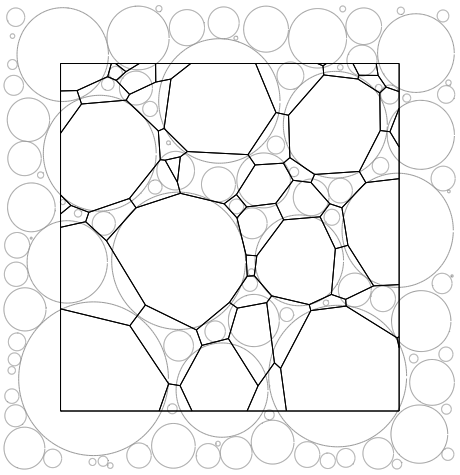

Figure 5: Cell structure around the circles within the RVE.

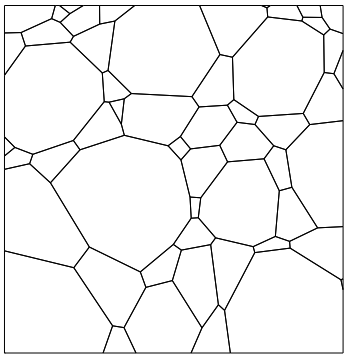

Figure 6: RVE with 'modified' Voronoi diagram.

In a third step a Delaunay triangulation for the circle center points is computed. Based on that triangulation the positions of 'modified' Voronoi points are calculated for each triangle following Figure 4. Assuming a triangle (123) is constructed by the center points of circles 1 to 3. First each triangle edge is divided into two parts proportional to the relation of radii belonging to the circles of edge vertices. Exemplary the edge connecting the center points of circles 1 and 2 is divided by the division point d_{12} at a distance of l_1 :

$$l_1 = \frac{r_1\, l}{r_1 + r_2} \tag{6}$$

from circle center 1 to circle center 2. l is the distance between center points of circles 1 and 2. r_1 and r_2 are the radii of circles 1 and 2. Second the edge division points d_{12}, d_{23} and d_{13} of triangle (123) define a new triangle for which the centroid V can be computed. Point V is the 'modified' Voronoi point of triangle (123).

In a fourth step all 'modified' Voronoi points inside the RVE bounds are connected according to a 'classical' Voronoi procedure. Finally the 'modified' Voronoi structure is cut along the RVE bounds. The resulting geometrical grain structure inside the RVE is illustrated in Figures 5 and 6. A comparism with the 'classical' Voronoi cell diagram in Figure 1 shows significant differences especially with respect to the grain size distribution.

The circles in the box do not fill the complete area of the cell structure. This results in a modified grain size distribution of the final cell structure compared to the initial size distribution of circles. Consequently an adaption is necessary for the free parameters of the distribution function, which has been used to generate the circle diameters d_j to obtain a cell structure corresponding to a predefined grain size distribution. Exemplary, a cell structure with median value $d_{50} = 0.94\mu m$ and standard deviation $\sigma_d = 0.78$ as measured in thin layer aluminum by [5] shall be generated. In order to obtain this cell structure the circle diameters are generated according to a cumulative lognormal distribution function with adapted values $\overline{d}_{50} = 0.66\mu m$ and $\overline{\sigma}_d = 1.40$. The parameters are adapted by an iterative fitting procedure. The resulting grain size distribution shows good agreement with the predefined cumulative lognormal distribution function (Figure 7). An example of the generated cell structure is illustrated in Figure 6. In principle it is possible to reproduce any arbitrary grain size distribution with high accuracy by the proposed algorithm.

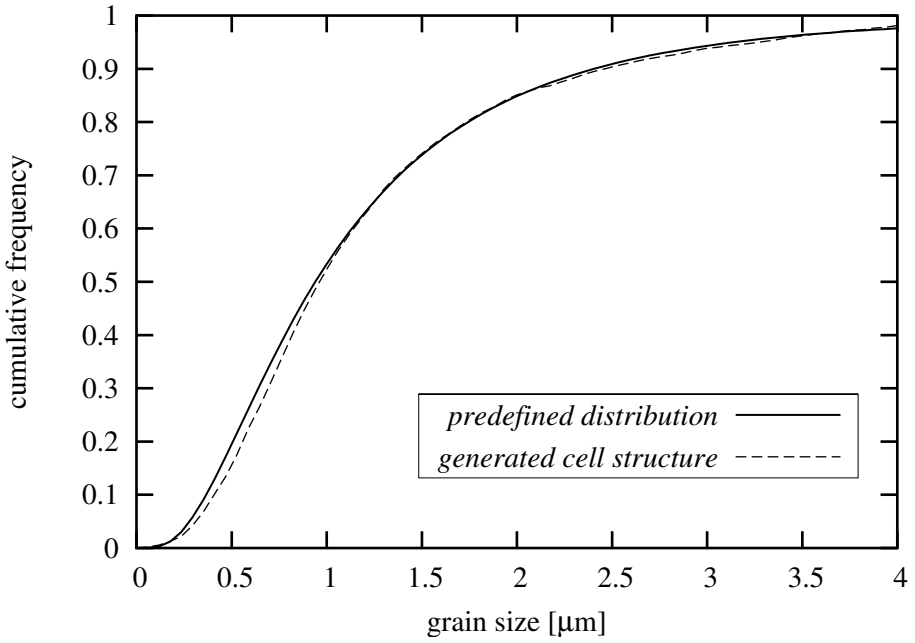

Figure 7: Comparison of predefined cumulative lognormal distribution function and resultig grain size distribution of generated cell structure.

3 MATERIAL MODELS ON THE MESOSCALE

In the next step the grains are discretized by triangular finite elements with quadratic shape functions. Additionally 6 node interface elements are assigned to the boundaries between single grains. Following Iesulauro and Ingraffea [1, 2, 3] an orthotropic material model is applied to the grain elements and a coupled cohesive zone model is assigned to the interface elements.

3.1 Grains

In order to take into account the dependency of material properties on crystal orientation, an orthotropic linear elastic material model and alternatively an orthotropic elastic plastic material model is assigned to the single crystals. However, the extension to the elastic plastic material model with realistic plasticity properties taken from [1] has shown no relevant improvements compared to the linear elastic model. The material properties requiered to describe the orthotropic linear elastic material behavior in the plane stress case are the Young's modulus E_1 and E_2, the Poisons ratio ν_{12}, and the shear modulus G_{12}. In the case of plastic behavior a flow rule of Hill plasticity is implemented with additional parameters of yield stress. The crystal orientation in plane is defined by a random angle $0 \leq \beta \leq \pi$ as illustrated in Figure 8.

3.2 Grain Boundaries

A coupled cohesive zone model (CCZM) is assigned to the interface elements to simulate crack propagation along grain boundaries. Cohesive zone models were originally introduced exemplary by [8] to describe the damage in the plastic zone of a crack by a traction-displacement relation. The traction-displacement relation of the currently used CCZM is shown in Figure 9. Therein the peak strength t_p of the CCZM depends directly on the missorientation $\Delta\beta$ between

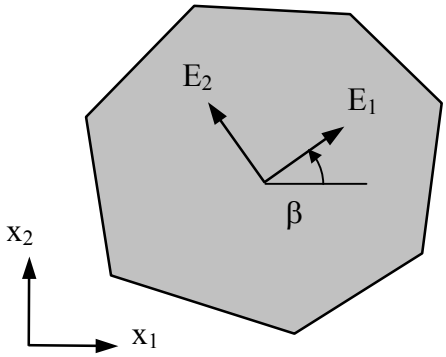

Figure 8: Orientation of orthotropic material axis in one grains.

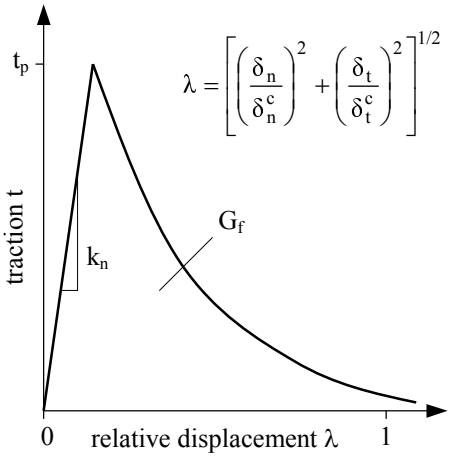

Figure 9: Coupled cohesive zone model of grain boundaries.

neighbouring single crystals:

$$\begin{aligned} \Delta\beta &= \beta_1 - \beta_2 \\ t_p(\Delta\beta) &= {t_p}^{avg} + \Delta t_p \, cos(4 \cdot \Delta\beta), \end{aligned} \tag{7}$$

where β_1 and β_2 indicate the orientations of two crystals along a common boundary. ${t_p}^{avg}$ is the average value of peak strength and Δt_p is the maximal peak strength deviation. The applied CCZM is sufficiently defined by the initial normal stiffness k_n, the peak strength t_p, the localized fracture energy G_f, and the ratio between critical interface openings δ_n^c in normal direction and δ_t^c in tangential direction [9]. The coupling of the interface opening in normal direction δ_n and the relative tangential slip of the two interface surfaces δ_t is realized by introducing a relative displacement λ according to Tvergaard [10]. The relation for λ is given in Figure 9.

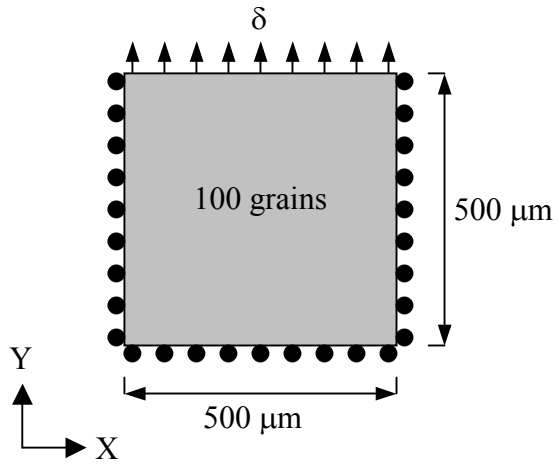

Figure 10: Boundary and loading conditions of tensile test.

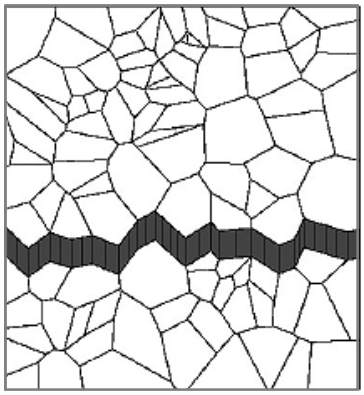

Figure 11: Example of simulated crack propagation on the mesoscale published in [1] by Iesulauro.

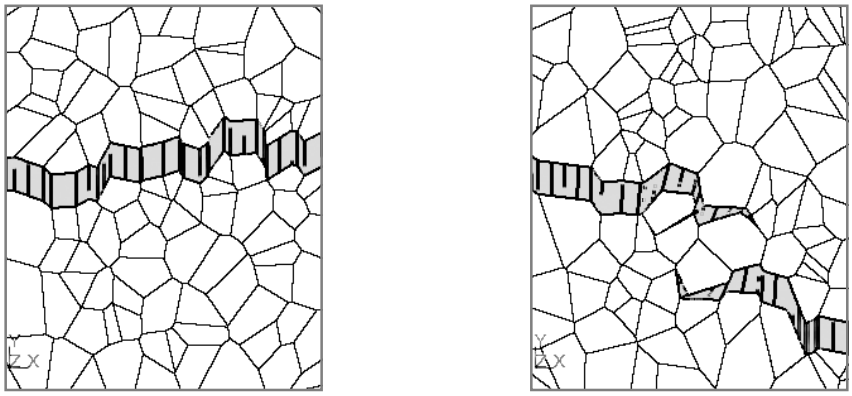

Figure 12: Two representative examples of simulated crack propagation showing the deformed state at 1% strain. Cracks (grey) are indicated by interface opening. The polycrystal cell structure is generated by the 'classical' Voronoi algorithm.

4 EXAMPLES

As a first example a displacement controlled tensile test is simulated on a two dimensional aluminum polycrystalline structure, following Iesulauro [1], to evaluate the model. Therefor 'classical' Voronoi cell structures as used in [1] are generated. Boundary conditions and geometrical dimensions of polycrystal RVE are represented in Figure 10. The same material properties as in [1] are assigned to single grains using the orthotropic linear elastic model. In the numerical analysis both, crystal orientation and material propertis of each crystal are distributed by normal distribution. The applied CCZM differs from the one that was used in [1] only by a more complex decohesion path. However, the material properties are chosen similar. All parameter values needed for the tensile test are summarized in Table 1. The standard deviation σ_d is applied to Young's modulus E_1 and E_2, as well as to the shear modulus G_{12}.

crystals	interfaces
$meanE_1 = 72000\,MPa$	${t_p}^{avg} = 500\,MPa$
$meanE_2 = 42000\,MPa$	$\Delta t_p = 0.05\,t_p^{avg}$
$meanG_{12} = 26900\,MPa$	$k_n = 4e7\,MPa$
$\sigma_d = 0.05$	$G_f = 0.15\,N/mm$
$\nu_{12} = 0.33$	$\frac{\delta_n^c}{\delta_t^c} = 1$
$0 \leq \beta \leq \pi$	

Table 1: Material and stochastic parameters of tensile test for aluminum specimen.

The tensile test was applied to initially undamaged samples. Figure 12 shows representative results for two generated samples of the deformed polycrystalline structure after tensile test. The crack initiation and propagation is reproduced by an opening of the interface. The complexity of crack formation in our simulations depends on both, the geometry of cell structure as well as the distribution of material parameters and crystal orientation. The mean value ${\sigma_t}^{poly}$ of the effective tensile strength calculated by 100 RVE samples is ${\sigma_t}^{poly} = 442\,MPa$. Therewith ${\sigma_t}^{poly}$ is lower than the average peak strength of the CCZM and yields a value which is reasonable. Altogether the simulated tensile tests on mesoscale qualitatively match the results of

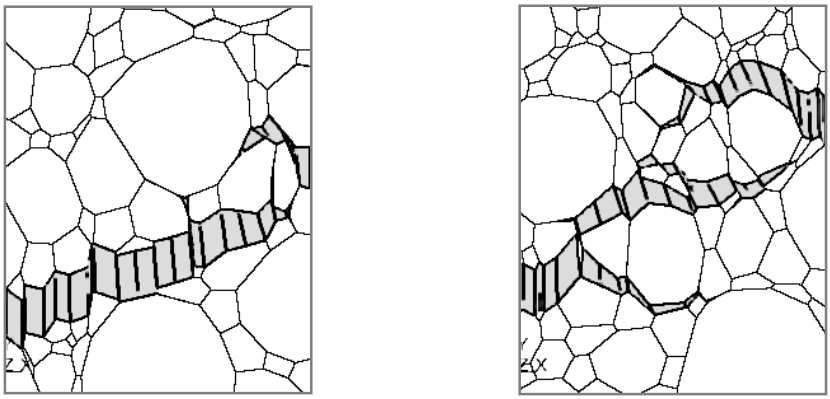

Figure 13: Two representative examples of simulated crack propagation showing the deformed state at 1.5% strain. Cracks (grey) are indicated by interface opening. The polycrystal cell structure is generated by the 'modified' Voronoi algorithm.

Iesulauro [1]. For comparison Figure 11 shows a crack path in a sample simulated by Iesulauro [1].

In a second study the damage behavior of aluminum samples generated by the 'modified' Voronoi algorithm was investigated. The free distribution parameters of the predefined lognormal distribution were chosen according to [5]: $d_{50} = 0.94\mu m$ and $\sigma_d = 0.78$. Consequently the sample size is adapted to $10\mu m$ in relation to the decreased grain size compared to the previous example. The principle boundary and loading conditions remained unchanged as well as the material properties (Table 1). First simulations using the more realistic polycrystal structure have shown a higher complexity in crack formation (Figure 13).

5 OVER-ALL MULTISCALE CONCEPT

In order to take into account that the physical process of damage simultaneously proceeds on multiple length scales the mesoscale model is part of a multiscale concept for damage analysis in polycrystalline materials. On the macroscopic scale the accumulating damage can be captured by an anisotropic damage tensor. Following the concept of hierarchical multiscale models the parameters of the damage tensor shall be evaluated by successive homogenization on RVEs of meso- and microstructure. Therewith it is possible to integrate the physical material effects, which are leading to crack initiation as well as crack propagation, into the damage model. The principle concept of a multiscale simulation strategy for polycrystalline materials is illustrated in Figure 14.

Based on the presented mesoscale model the next research step within the multiscale concept is focused on the determination of constitutive relations for the CCZM from mixed continuum atomistic simulations performed on RVEs on microscale. The microscale results shall be subsequential homogenized to the mesoscale. Therefor, first investigations of atomic debonding along grain boundaries are done based on the quasicontinuum method developed by Tadmor [11]. Based on atomistic energy laws this method allows a reproduction of atomic debonding as the source of micro crack initiation in zones of localized damage. In undamaged model regions conventional continuum mechanical formulations are applied to calculate the struc-

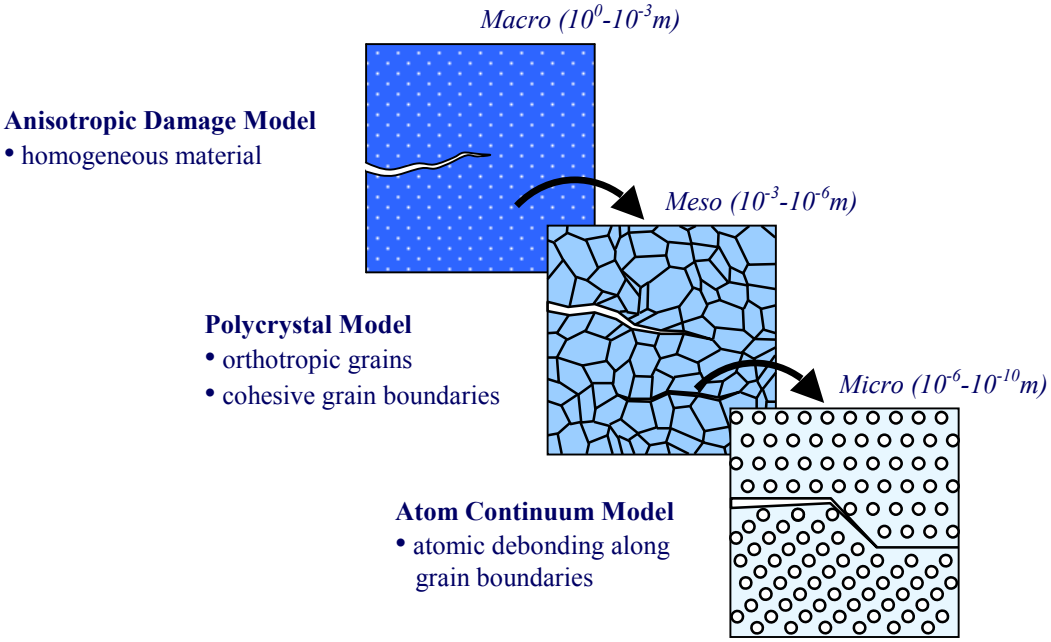

Figure 14: Hierarchical multiscale model for polycrystalline materials.

tural response. During the simulation zones of atomistic resolution are adapted following the progress of damage. Therewith the method allows a significant reduction of degrees of freedom compared to pure atomistic methods, such as molecular dynamics, and ensures a high accuracy on the atomic level at the same time.

6 CONCLUSIONS

The proposed polycrystal model enables the simulation of crack formation in statically loaded two dimensional polycrystalline mesostructures without the necessity of initial damage definition as necessary in classical linear elastic fracture mechanic approaches. A main advantage of our mesoscale model is the underlying realistic polycrystal structure. This structure shows a better fit to measured grain size distribution in polycrystalline materials compared to often used 'classical' Voronoi diagrams. In principle the presented 'modified' Voronoi algorithm is able to generate polycrystal structures with arbitrary predefined grain size distribution.

However, up to now the improved model is limited to two dimensions and can not cover effects of damage evolution in 3D. Hence, the current work is concentrated on the extension of the introduced polycrystal model to three dimensions. Furthermore based on the quasicontinuum concept [11] the future research work has to focus on the development of a 3D mixed continuum atomistic model on the microscale at finite temperature to realistically simulate the atomic debonding along grain boundaries and homogenize the material behavior of micro RVE to describe the decohesion on the mesoscale.

REFERENCES

[1] E. Iesulauro, *Decohesion of Grain Boundaries in Statistical Representations of Aluminium Polycrystals*. Master Thesis, Cornell University, 2002

[2] E. Iesulauro, A. R. Ingraffea, S. Arwade and P. A. Wawrzynek, Simulation of Grain Boundary Decohesion and Crack Initiation in Aluminium Microstructure Models. W. G. Reuter and R. S. Piascik eds. *Fatigue and Fracture Mechanics: 33rd Volume*, ASTM, West Conshohocken, PA, 2002.

[3] A. R. Ingraffea, E. Iesulauro, K. Dodhia and P. A. Wawrzynek, A Multiscale Modeling Approach to Crack Initiation in Aluminum Polycrystals. H. A. Mang, F. G. Rammerstorfer and J. Eberhardsteiner eds. *Fifth World Congress on Computational Mechanics*, WCCM V, Vienna, Austria, 2002.

[4] F. Aurenhammer, Voronoi Diagrams - A Survey of a Fundamental Geometric Data Structure. *ACM Computing Surveys*, **23**(3), 345–405, 1991.

[5] S. Kirchner, *Ausscheidungshärtung dünner Al-0,6Si-0,6Ge-Schichten: Studie zur ertragbarkeit eines Massivmaterial-Legierungskonzeptes*. Dissertation, University Stuttgart, 2001.

[6] C. V. Thompson, Grain Growth in Thin Films. *Annual Review of Materials Science*, **20**, 245–268, 1990.

[7] W. Fayad, C. V. Thompson and H. J. Frost, Steady-State Grain-Size Distributions Resulting from Grain Growth in Two Dimensions. *Scripta Materialia*, **40**(10), 1199–1204, 1999.

[8] D. S. Dugdale, Yielding of Steel Shields Containing Slits. *Journal of the Mechanics and Physics of Solids*, **8**, 100–104, 1960.

[9] J. F. Unger and C. Könke, Simulation of concrete using the Extended Finite Element Method. N. Bicanic, R. de Borst, H. Mang, and G. Meschke eds. *Proceedings of EURO-C 2006, Computational Modelling of Concrete Structures*, 2006.

[10] V. Tvergaard, Cohesive zone representations of failure between elastic or rigid solids and ductile solids. *Engineering Fracture Mechanics*, **70**, 1859–1868, 2003.

[11] E. B. Tadmor, *The Quasicontinuum Method - Modeling Microstructure on Multiple Length Scales: A Mixed Continuum Atomistic Approach*. Ph. D. Thesis, Brown University, 1996